PHYSOR 2018: Reactor Physics paving the way towards more efficient systems
Cancun, Mexico, April 22-26, 2018

CORE SAFETY MEASURES IN ESFR-SMART

A. Rineiski[1], C. Meriot[2], M. Marchetti[1], and J. Krepel[3]

[1]Karlsruhe Institute of Technology (KIT)
KIT/IKET, Campus Nord, B. 421, 76344 Eggenstein-Leopoldshafen, Germany

[2]EDF-R&D, EDF Lab Paris-Saclay
7 Boulevard Gaspard Monge, 91120 Palaiseau, France

[3]Paul Scherrer Institut (PSI)
5232 Villigen, Switzerland

andrei.rineiski@kit.edu, clement.meriot@edf.fr, marco.marchetti@kit.edu, jiri.krepel@psi.ch,

ABSTRACT

A new EURATOM project, ESFR-SMART, started in September 2017. It follows an earlier project, CP-ESFR, on a commercial-size European Sodium Fast Reactor (ESFR). ESFR-SMART is devoted to ESFR safety and related studies, including new reactor core safety measures, in particular reduction of the sodium void reactivity effect. A "low void" core is expected to show a better safety behavior with respect to the CP-ESFR one. The core optimization has been performed in two steps. A preliminary configuration was established at KIT by assessing several designs, taking into account earlier studies on ESFR and ASTRID cores. Compared to the initial ESFR case, the sodium void effect is reduced by introduction of the sodium plenum above the core and reduction of the fissile core height compensated by its radial extension. In the inner core, the fissile region is shorter, while the lower fertile blanket is longer as compared to those in the outer part. Passive safety devices are foreseen to prevent core degradation. Corium transfer tubes are introduced to avoid re-criticalities after a hypothetical accident. A core reloading scheme for this configuration was developed at PSI.

Then, a fine optimization of this design has been performed at EDF with an in-house multi-physics and multi-objective optimization tool called SDDS. The calculated void effect in the region including the core and plenum at the end of cycle has been reduced by 80% to a fraction of the beta-effective value while achieving a near-zero breeding gain and keeping a relatively simple axial configuration. Moreover, the selected core seems to have a satisfying behavior during both Unprotected Loss Of Service Station Power and Unprotected Control Rod Withdrawal hypothetical accidents.

Further optimization studies of the control rod design and the passive safety devices will be conducted, as well as Monte-Carlo neutronics calculations. The improved safety behavior should be confirmed by further analyses foreseen in ESFR-SMART.

KEYWORDS: Sodium fast reactor, reactor safety, sodium void effect, corium transfer tubes

1. INTRODUCTION

A large 3600 MWth European Sodium Fast Reactor (ESFR) was studied in the CP-ESFR project in the late 2000s and early 2010s [1]. Then EURATOM Sodium Fast Reactor (SFR) activities were mainly conducted on ASTRID in the ESNII+ project [2]; ASTRID is a 1500 MWth French SFR design [3]. In September 2017, the ESFR-SMART project started [4] on a 3600 MWth core, including an activity on ESFR core safety measures.

The initial ESFR design, referred hereafter as ESFR Working Horse (ESFR-WH), was proposed by CEA [5]. Compared to earlier European large SFR projects, the pin diameter and fuel volume fraction are higher, the Pu enrichment is smaller, see Table I. The numbers of fuel assemblies (FAs) in the inner and outer cores are 255 and 228, respectively. The breeding gain is near-zero, the axial blankets and radial reflector contain no fertile material, that is replaced by steel. The sodium void reactivity effect (SVRE) is smaller in ESFR-WH compared to earlier large European designs, but definitely positive: near 3$ at the beginning of life (BOL), about 2$ higher at the end of equilibrium cycle (EOEC), 1$ being about 400 pcm. Optimization studies in CP-ESFR led to a modified design named ESFR-CONF2. The radial layout is the same as in ESFR-WH, but the axial one was changed: in the region above the core, a large sodium plenum of 60 cm topped by an absorber layer was implemented replacing the upper steel blanket and some above structures; in addition a fertile blanket was introduced below the core instead of the steel one [6], see Figure 1. In Figure 1 (right) the dimensions for FA axial sub-regions are given in mm. The extended SVRE in ESFR-CONF2, i.e. including the plenum void effect, was reduced to about 1$ at BOL; see Table II with MCNP and ERANOS results [6]. The extended region is considered because coolant boiling in the core extends to the plenum above.

Table I. Main ESFR-WH parameters

Number/Enrichment of Inner FAs	225/14.6%wt
Number/Enrichment of Outer FAs	228/17.0%wt
Control and Shutdown Device (CSD)	24
Diverse Shutdown Devices (DSD)	9
Target Fuel residence time (EFPD)	2050
Target Burn-up (GWd/t)	100
Fissile core height (cm)	100
HEX FA pitch (mm)	210.8
Fuel Pellet Diameter (mm)	9.43
Pin (outer clad) diameter (mm)	10.73
Pins per S/A	271

Table II. Void effect at BOL in ESFR-WH and ESFR-CONF2 computed with JEFF 3.1 data

	ESFR-WH, ERANOS	ESFR-CONF2, ERANOS	ESFR-CONF2, MCNP
Extended SVRE, pcm	1211	496	422

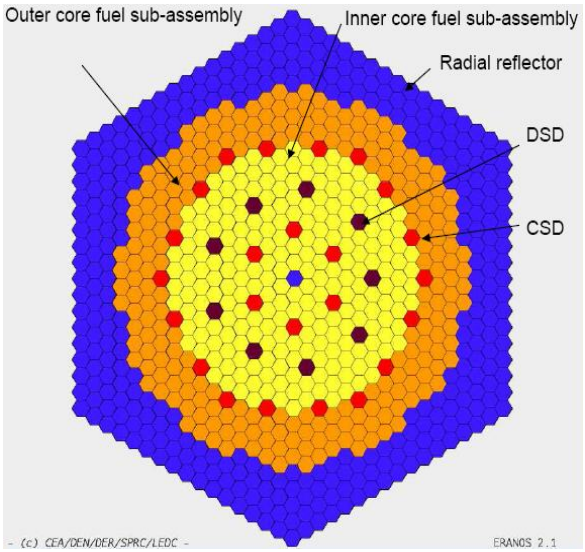

Head	230
Reflector	276
Absorber	282
Plug	18
Na Plenum	600
Plug	18
Upper gas plenum	50
Active core	1000
Lower blanket	300
Lower gas plenum	913
Plug	82
Foot	370

Figure 1. ESFR-WH/ESFR-CONF2 layout in plane (left) and ESFR-CONF2 axial FA layout (right)

The transient simulations show [6] that in ESFR-CONF2 the reactivity is lower compared to that in ESFR-WH at the sodium boiling onset because of a negative sodium void effect in the plenum, thus leading to a smaller power peak at this time. On the other hand, SVRE is definitely positive in ESFR-CONF2 at EOEC, about 3$. Therefore a further SVRE reduction is of interest.

In CP-ESFR, introduction of corium transfer tubes was proposed, but the related safety analyses were limited. An ASTRID design with transfer tubes was considered in ESNII+. This design also includes passive safety devices, such as Curie-point rods and hydraulically suspended absorber rods introduced in the core in case of a high coolant temperature and strong reduction in the coolant flow, respectively. The earlier ESFR and ASTRID studies are considered for introducing ESFR-SMART core safety measures.

The ESFR-SMART design proposal was prepared in two steps. The first step was to establish a preliminary configuration; the second step was to perform optimization studies.

2. PRELIMINARY CONFIGURATION

The preliminary configuration was established by taking into account the earlier studies. A particular feature of the ASTRID core is its heterogeneous design. The boundary between the inner core and sodium plenum is at a lower location than that in the outer core, while the boundary between the fuel and lower blanket is the same in the inner and outer cores [3]. An internal axial fertile blanket is introduced into the short inner core.

While taking ESFR-CONF2 as a starting point for ESFR-SMART establishment and trying to assess the applicability of the ASTRID approach for SVRE reduction, several ASTRID-like layouts were assessed at KIT (see Figure 2): M0 that is similar to ASTRID, M1 obtained from M0 by moving the inner fertile blanket downwards, M2 obtained from M1 by moving the boundary between fissile and fertile in the inner core upwards. In M1 and M2, the total height of the inner fissile is the same as that in M0, the outer core being not modified compared to M0. The amount of fertile is the highest in M2.

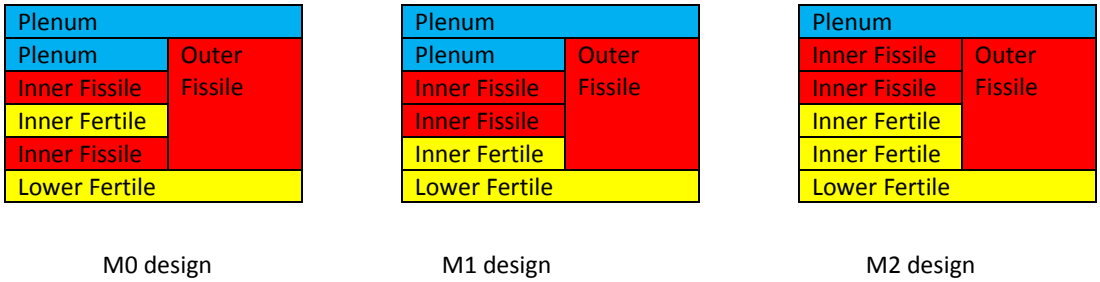

Figure 2. ASTRID-like and modified axial SFR layouts.

The lowest extended SVRE value (while considering the voided region above the Lower Fertile) was obtained for the M2 design. One may treat the transition from M0 to M2 as introduction of a radial internal blanket instead of the axial one, the neutron leakage being enhanced in both cases compared to conventional designs. Note that the presence of the inner fertile blanket in M0 may lead to a positive reactivity introduction after a hypothetical accident leading to fissile melting followed by blanket relocation. A lower upper fissile boundary in the inner core - as compared to that in the outer one - may also influence the performance of control rods. Thus, an M2-type axial layout has been chosen for the ESFR-SMART preliminary configuration, the inner and outer core heights being 80 and 100 cm, respectively. The same FA axial layout as in CONF2 was adopted for the preliminary configuration above the upper fissile boundary and below the lower blanket.

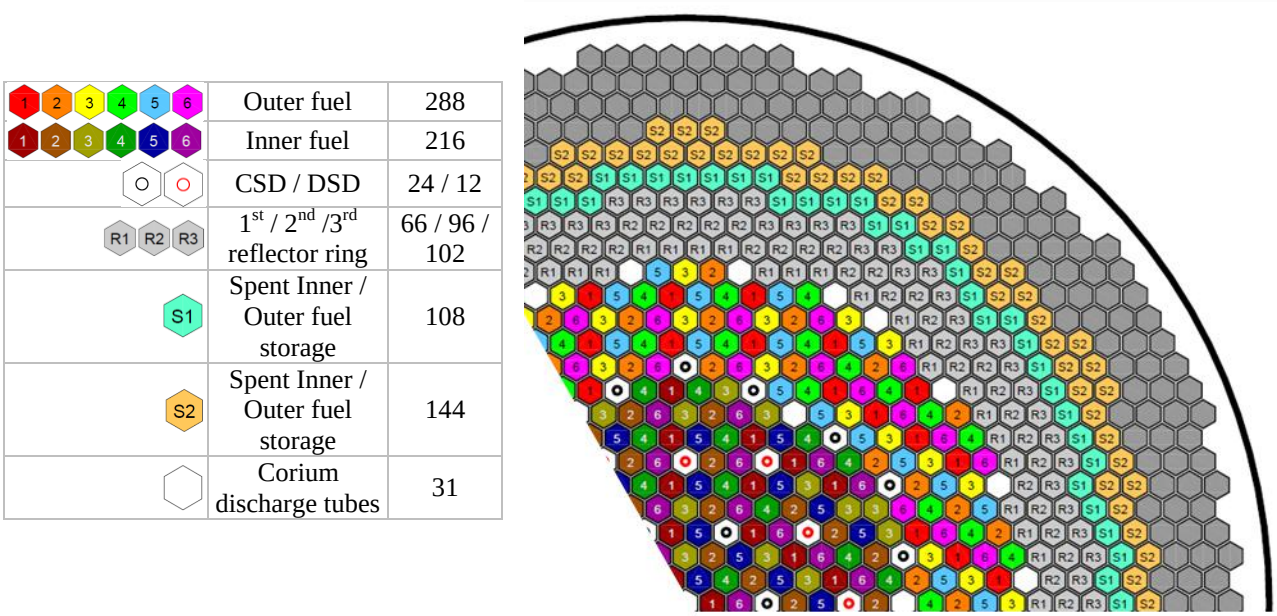

Figure 3. ESFR-SMART radial layout and reloading scheme (120° symmetry).

In view of a smaller fissile volume in the inner core, FAs were added at the core periphery, see Figure 3. The numbers of inner and outer core FAs in ESFR-SMART are fixed to 216 and 288, respectively. In Fig. 3 also the numbers of fuel batches in the equilibrium cycle are shown for a 6-batch reloading scheme developed at PSI. Note that the total fissile volume is slightly increased in the preliminary configuration, compared to ESFR-WH/CONF2, meaning that mean linear power in this configuration is smaller.

It is known, that a smaller height-to-diameter ratio makes the void effect smaller. A core height reduction in the inner core is more efficient compared to that in the outer core. Therefore in the design shown in Fig. 3, the inner fissile core is shorter than the outer one. Another advantage of the shorter inner core is that the enrichments in the inner and outer cores can be the same, provided that the core heights and numbers of FAs are chosen while taking into account this purpose. Single enrichment facilitates fuel fabrication. For the preliminary configuration, single fuel enrichment of 17% was chosen.

Figure 3 also shows the locations of corium transfer tubes. These tubes are similar to FAs at axial locations where absorber is placed above the plenum. The space within can-wall below the absorber is occupied with coolant. The lower part of the tube is preliminary assumed to be connected to the core catcher region. One of currently considered options - to make possible a slight coolant circulation through the tubes for cooling the absorber at their upper parts - is to make a connection between the core catcher region and the high pressure plenum below FAs, with a relatively high pressure drop between these regions under operating conditions. The DSD locations can be fully or partly occupied by passive safety devices. The reflector rings 1 and 2 are with steel “pins”, similar to ESFR-WH, while reflector ring 3 includes neutron absorber to decrease the influence of spent FAs located next to the third reflector ring on core reactivity. In total the numbers of spent FAs in the internal storage are 108 and 144, respectively.

In ESFR-CONF2, the height of the lower axial blanket is 30 cm. If fertile is also introduced in the lower part of the inner core, its amount increases. For both initial and increased fertile amounts, the breeding ratio is positive. If a near-zero breeding gain is targeted, the lower blanket should partly contain fertile and partly steel, that may increase SVRE. The fertile region optimization is addressed in the next section, fertile blankets of 5 cm were proposed for the preliminary configuration. Thus, the preliminary configuration deviates from the M2 layout: the lower fertile boundaries differ in the inner and outer cores.

3. OPTIMIZED CONFIGURATION

The SDDS method, developed at EDF, has been used to perform a fine optimization of the preliminary configuration. The goals were to reduce the extended SVRE and achieve a near-zero breeding gain, while keeping a relatively simple design and reducing the core diameter as much as possible.

Usually, optimization studies are led step-by-step, parameter after parameter, at first with neutronics calculation codes, then with thermal-hydraulics and thermal-mechanics evaluations. After a modification of the design, this process is repeated. This is a time-consuming methodology, which does not ensure to catch the global optimum for a set of performances in a parametric space. SDDS method aims to help the designer by giving him an overall perspective. It provides a multi-physics analysis, dealing with neutronics, thermal-hydraulics and fuel performances simultaneously, and covers a very large parametric space, so that no design is let aside. The general layout of the process is given on Figure 4.

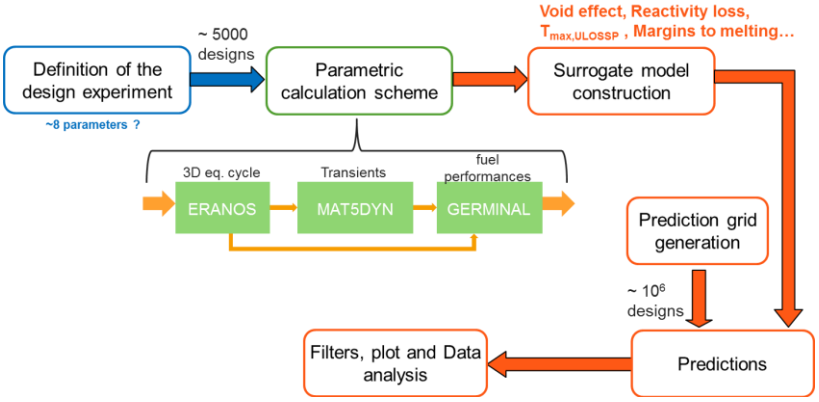

Figure 4. General layout of the SDDS method.

3.1. Design of experiment

The radial layout and reloading scheme are kept identical for the whole optimization study: they are the same for each considered trial configuration of the design of experiment (set of configurations), see Figure 3. First, 8 parameters have been chosen related to the axial (see Figure 5) and internal structure of FAs:

- a fertile plate of variable height and position has been considered in the inner FAs. Increasing the fertile plate height (F) reduces the inner steel blanket height in order to maintain a reasonable fissile region height;
- an Inner/Outer (D) upper offset with a variable height is considered at the top of the active core;
- the outer core height (H);
- the pellet radius and the inner clad radius;
- the spacer wire diameter;
- the number of pins per FA;

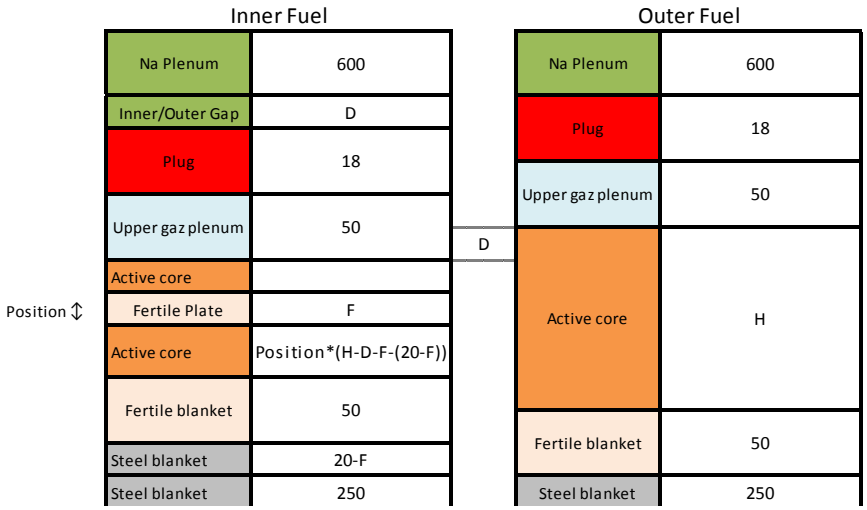

Figure 5. Axial structure of FAs and parameters used for the optimization

Some constraints have been added: as the increase of the fuel pellet inner hole radius is a win-win parameter for both ULOSSP and UCRW behavior, we maintain it equal to 1/3 of the pellet radius; as some parameters (dimension of the pins, number of pins per S/A) have an impact on the calculation of the S/A pitch and thus the core diameter, we limit the increase of the active core diameter to +10% of the initial core diameter of 5.5m. The ranges of variation of the parameters are given in table III.

Table III. Ranges of the parameters

Parameters	Initial design	Min	Max
Pellet radius (cm)	0.4715	0.3	0.5
Cladding inner radius (cm)	0.4865	0.35	0.5
Spacer wire diameter (cm)	0.1	0.08	0.12
Number of pins	271	271	331
Outer core height (cm)	100	90	130
Inner/Outer heights Offset (cm)	0	0	30
Fertile plate position (% of inner height)	0	0	50
Fertile plate height (cm)	0	0	20

A 5000-points design of experiment is created using entropy maximization methods [7], in order to maximize the dispersion of the points over the parametric space and improve the quality of surrogate models to be established afterwards.

3.2. Calculation scheme

The performances of each core configuration are evaluated with an ERANOS/MAT5DYN/GERMINAL [8, 9, 10] calculation scheme for neutronics/thermal-hydraulics/fuel performances analysis, respectively. The neutronics calculation scheme set up with ERANOS is composed of the following steps, to evaluate the performances of each design and feed the further transient and thermal-mechanics calculations:

- First, we adjust the plutonium content in the inner and outer cores for each design to ensure criticality at EOEC plus a reactivity margin set to 700 pcm and minimize the maximal sub-assembly power over the core. These calculations are performed with a neutron transport code in 3D geometry (VARIANT solver), with inserted control rods and following the mentioned fuel reloading scheme to achieve equilibrium. The 33-group cross-sections for neutron transport calculations are prepared with a cell module of ERANOS with a fine scheme for active zones (heterogeneous geometry, library with 1968 energy groups).
- The fuel depletion simulations until equilibrium and study of equilibrium cycle are performed.
- The feedback calculation uses a diffusion solver in 3D geometry except for sodium void worth and sodium expansion effect which are calculated with a transport code in 2D RZ geometry.
- Finally, a complete set of data for Unprotected Control Rod Withdrawal (UCRW) calculations is established using a neutron transport code in 3D geometry. The reactivity worth and power shape swing induced by each individual rod removal are evaluated.

MAT5DYN uses a multi-channel description, a simplified pin thermal evaluation, and a point kinetics neutronics model to simulate several transients: Unprotected Loss Of Flow (ULOF), Unprotected Loss of Heat Sink (ULOHS), Unprotected Loss of Service Station Power (ULOSSP), and Unprotected Transient Over Power (UTOP, simulated in order to determine relative elevations of core power due to reactivity insertions during UCRW transients). It uses a single-phase description of the coolant, and an extrapolation of the coolant temperature after reaching the boiling temperature. As we only perform comparative analyses, this approximation is suitable.

The thermal-mechanics calculations are performed with GERMINAL. The maximum linear power is taken from neutronics calculations. For each core configuration and for each cycle of its equilibrium campaign, the hottest sub-assemblies are simulated to determine the minimal margin to fuel melting at nominal conditions, and for each control rod withdrawal, the hottest fuel sub-assemblies are simulated to determine their linear power leading to fuel melting. The safety margin during UCRW is then evaluated as the difference between the linear power leading to fuel melting and the maximum linear heat rate at the end of the UCRW, considering the relative elevation of power calculated with MAT5DYN and uncertainties to ensure the non-melting with 95% confidence.

3.3. Creation of surrogate models

The data basis containing the performances of ~5000 core designs is used to build surrogate models with an interpolation method called Kriging [11] (also called Gaussian Process Regression). This method performs interpolation without fitting, which is a proper option for results provided by deterministic codes, and generates a meta-model for predicting performances of similar configurations. It also gives information about the quality (confidence interval) of the prediction of the meta-model, which is very useful to eliminate unrealistic designs from consideration. The quality is evaluated using an independent

set of designs (10% of the data basis).

After creating a first set of surrogate models, we realized that the quality of the prediction of the margin to melting at nominal conditions was very bad. In fact, the half of the data basis is composed by uninteresting designs that melt at normal operating conditions (see Fig. 6). Thus, we created a new set of 5000 designs, in which we prohibited negative margins to melting, by predicting their values for each core design with the first dataset.

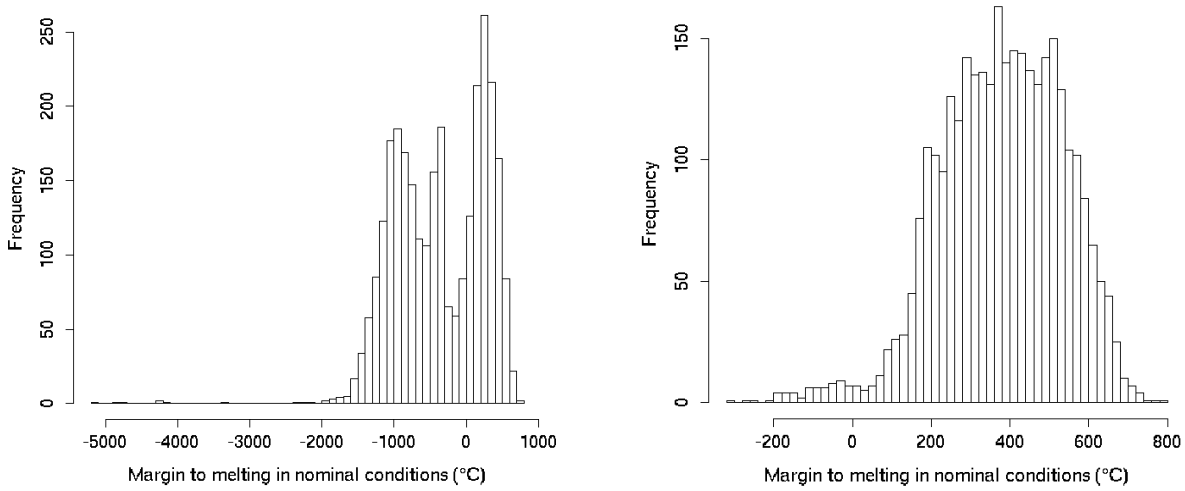

Figure 6. Distribution of the margins to melting in nominal conditions in the first (left) and optimized (right) data basis

Then, the entire process has been repeated (simulations and construction of a new set of surrogate models). The accuracy (95% confidence intervals) values of the main surrogate models after this second step are given in table IV.

Table IV. 95% confidence intervals for major performance indicators

Performance indicator	2σ (95%)
Extended Void effect (pcm)	91
Reactivity loss (pcm)	20
Nominal margin to melting (°C)	41
UCRW margin to melting (W/cm)	10
Maximal sodium temperature in ULOSSP (°C)	45
Breeding gain (%)	0.42

3.4. Predictions and selection

The performances of a large amount of cores (~1,5 million designs) distributed on a regular grid are evaluated with the surrogate models. Figure 7 presents the distribution of these designs in the (Maximal sodium temperature in ULOSSP, Margin to melting during UCRW) space (or (T_{ULOSSP}, δ_{UCRW})). First, we removed the non-viable cores, i.e. the ones that present a very low margin to fuel melting in nominal

conditions.

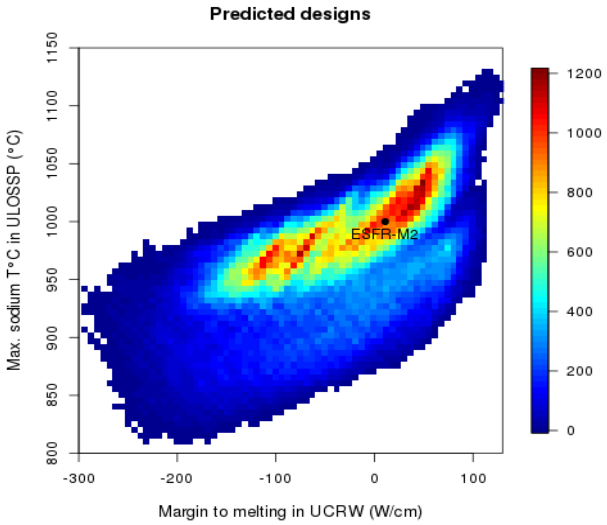

Figure 7. Distribution of the predicted designs in the (T_{ULOSSP}, δ_{UCRW}) space

The ULOSSP indicator is an evaluation of the maximal temperature of the sodium, with an extrapolation when it exceeds the boiling temperature. A positive margin to melting during UCRW (or δ_{UCRW}) is a guarantee of non-melting of the fuel during any UCRW transient at any time.

Then, we analyzed the distribution of the performances in this (T_{ULOSSP}, δ_{UCRW}) space and filter the most interesting designs. Figure 8 present the total void effect (SVRE at EOEC) of the predicted designs with a zoom on the interesting area of the space, where the margin to melting during UCRW is positive. In this visualization, the color of the pixel is indexed to the mean of the performance (or parameter) of the core designs in the pixel. As we can see, we can find designs on the (T_{ULOSSP}, δ_{UCRW}) Pareto front (bottom-right frontier of the colored surface) with a very low void effect.

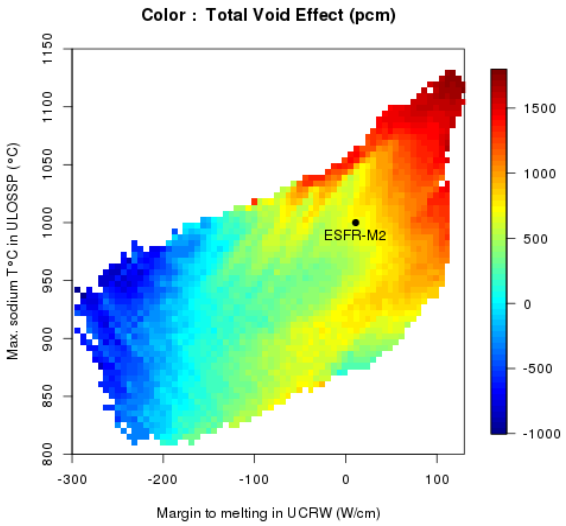

Figure 8. Distribution of the predicted designs in the (T_{ULOSSP}, δ_{UCRW}) space

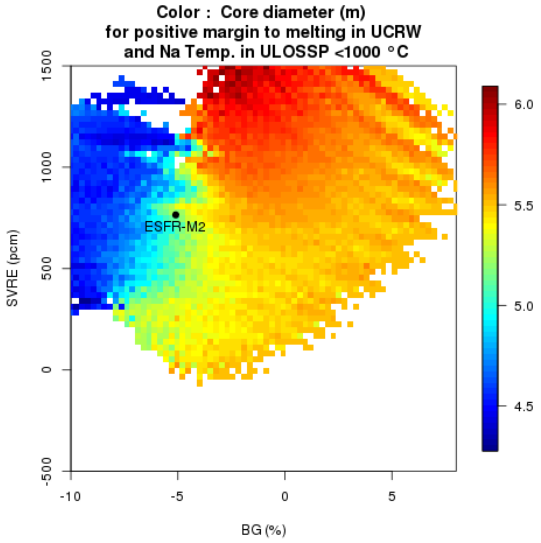

Figure 9. Distribution of the core diameter of the predicted designs in the (SVRE, BG) space

Figure 9 shows the distribution of the core diameter of the predicted designs in the (SVRE, Breeding Gain) space. Beforehand, we filtered the designs that had a negative margin to melting during UCRW and a bad behavior in case of ULOSSP. This illustration shows that it is not possible to reduce the core diameter if we target a near-zero breeding gain. Finally, designs that have a low void effect and a near-zero breeding gain have a core diameter around 5.5m, as well as the preliminary configuration.

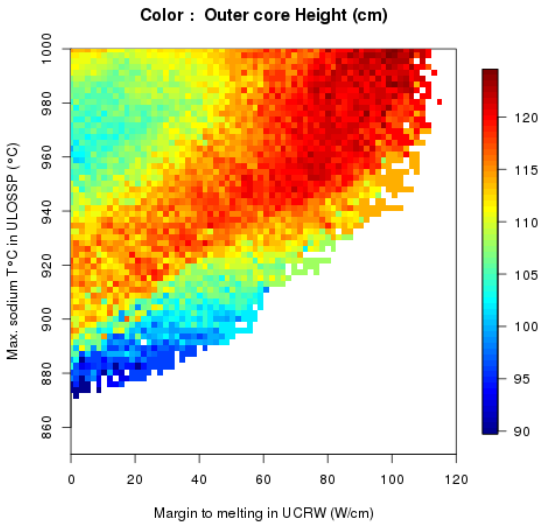

Figure 10. Distribution of the outer core height in the (T_{ULOSSP}, δ_{UCRW}) space

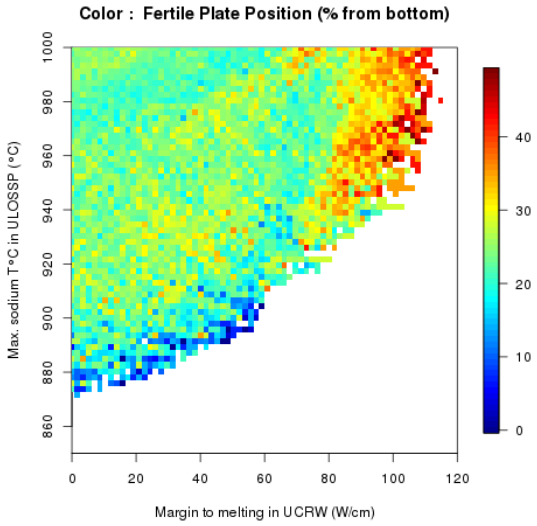

Figure 11. Distribution of the fertile plate position (in % of the inner fuel height) in the (T_{ULOSSP}, δ_{UCRW}) space

Some trends have been assessed while looking at the distribution of the parameters in the (T_{ULOSSP}, δ_{UCRW}) space (see example on figure 10 and 11):

- The position of the fertile plate changes along the Pareto front: a higher plate is preferable to reduce the axial power form factor and improve the UCRW behavior. In this study, it is preferable to have a low fertile plate, in order to reduce the sodium void effect. Moreover, it is possible to find designs with a low fertile plate and a positive margin to melting during ULOSSP.
- Adding an upper inner/outer height offset between 0 and 5cm improves both ULOSSP and UCRW behavior. Thus, it is possible to find designs with satisfying performances and no offset.
- The outer core height should be reduced to improve the void effect and thus the ULOSSP behavior. However, having a near-zero breeding gain implies to have a height higher than 95cm for these designs.
- The pellet diameter must be reduced.
- The spacer wire diameter should be reduced: it is a win-win parameter for both ULOSSP and UCRW. However, for reasons of technical feasibility of the assembly, we decided to maintain the wire/pin diameter ratio above 0.09, as it was the case in CP-ESFR.
- The optimal value for the pellet-cladding gap is around 0.015 for these designs.

To select the most optimized designs among the predictions, we capture the successive Pareto fronts (lower right boundary on figure 8) and exclude the cores with a too low (<-2%) breeding gain, a too large diameter, or a negative margin to melting in case of UCRW. Then, we measure the performances of this set of selected designs with the ERANOS/MAT5DYN/GERMINAL scheme, to eliminate the prediction error of the surrogate models.

The design with the lowest void effect and a near-zero breeding gain was obtained (A in table V), but the

selected design (B) was chosen after filtering the data basis to respect some constraints of the project: **design B is the core that presents the lowest void effect, with a low fertile plate, a unique Pu content, no inner/outer height offset, and a pooling of the axial elevations of the inner and outer FAs to simplify the axial structure.** Compared to the preliminary configuration, a reduction of 80% of the total void effect has been performed, while achieving a near-zero breeding gain and slightly reducing the assembly pitch. Note that the selected configuration is similar to the M2 layout (see Figure 2).

Table V. Performances of the preliminary and optimized designs

	Preliminary	A	B (Selected)
Inner Enrich. (%vol)	17	17.86	17.32
Outer Enrich. (%vol)	17	16.93	17.32
Cycle length (EFPD)	2195	2170	2170
Breeding Gain (BOEC)	-5.2%	-0.9%	-0.5%
Extended SVRE (pcm) at EOEC	765	20	153
Estimated max. Na T in ULOSSP (°C)	>1000 (extrapolation)	761	880
Minimal Margin to melting in UCRW (W/cm)	11	27	23
Outer fiss. Height (cm)	100	102.5	95
Inner fiss. Height (cm)	80	67.5	75
Outer/Inner Offset (cm)	0	15	0
Fertile plate height (cm)	-	17.5	20
Fertile plate lower bound. in the inner fissile(cm)	-	0.0	0.0
Fertile blanket height (cm	5	5	5
Inner core steel blanket (cm)	45	27.5	25
Pellet radius (cm)	0.4715	0.4680	0.4680
Cladding inner radius (cm)	0.4865	0.4835	0.4835
Fuel pellet inner hole radius (cm)	0.125	0.156	0.156
Wire diameter (cm)	0.10	0.10	0.10
Assembly Pitch (cm)	21.08	20.985	20.985

4. CONCLUSIONS

A new EURATOM ESFR-SMART project started recently, including an activity on core safety measures. First, a new preliminary core configuration has been established by taking into account earlier studies on ESFR and ASTRID, in particular on sodium void effect reduction. The radial core layout and 6-batches reloading scheme have been fixed, particularly aiming to limit power discrepancies and reactivity variations between batches, to include corium discharge tubes and an internal storage for irradiated fuel.

Then, the optimization of the axial structure and pin geometry has been performed with the multi-physics and multi-objectives tool SDDS. A wide parametric space has been studied through the use of surrogate models to predict the neutronics, thermal-hydraulics and thermal-mechanics performances of a large number of cores. An optimized but relatively simple core design has been selected, with a reduced calculated SVRE (under 0.5$ at end of equilibrium cycle) and a near-zero breeding gain.

Thus, it appears feasible to reduce the sodium void reactivity effect to a near-zero value, while incorporating corium transfer tubes and passive safety devices. The proposition of the selected core design is a building block of the ESFR-SMART project. It will be complemented by a number of studies starting from further optimization of the control rods and passive safety devices, as well as Monte-Carlo

neutronics calculations for checking the results obtained with deterministic codes. More detailed fuel, thermal-hydraulics, and coupled simulations will be done. The described safety measures should improve core behavior under hypothetical accident conditions that should be confirmed by analyses foreseen in ESFR-SMART.

ACKNOWLEDGMENTS

The research leading to these results has received funding from the EURATOM research and training programme 2014-2018 under grant agreement No 754501. The first author thanks F. Gabrielli, KIT, for providing results of ERANOS calculations for ASTRID-like models. The second author wants to thank EDF colleagues: F. Barjot and D. Schmitt for their help on SDDS and E. Girardi, S. Massara and S. Poumerouly for their assistance during the definition of the set of trial configurations and their analysis.

REFERENCES

1. G. L. Fiorini et al., “EC - 7th Framework program, CP-ESFR”, FISA 2009, June 22-24, 2009, Prague
2. A. Vasile et al., "The European Project ESNII Plus", ICAPP 2015, May 3-6, 2015, Nice
3. P. Le Coz, “The ASTRID Project: Status and Future Prospects”, FR13, 4-7 March, 2013, Paris.
4. K. Mikityuk et al., “ESFR-SMART: new Horizon-2020 project on SFR safety”, FR17, June 26-29, 2017, Yekaterinburg.
5. D. Blanchet et al., CEA, Personal communication, 2009.
6. A. Rineiski et al., "ESFR core optimization and uncertainty studies", FR13, 4-7 March, 2013, Paris.
7. M.C. Shewry and H.P. Wynn, “Maximum Entropy Sampling”, Journal of Applied Statistics, 14, pp. 165-170, 1987.
8. G. Rimpault et al., “The ERANOS code and data system for fast reactor neutronic analyses”, PHYSOR 2002, Seoul, October 7-10, 2002
9. S. Massara et al., “Dynamics of critical dedicated cores for Minor Actinide Transmutation”, Nuclear Technology, 149, pp. 150-174, 2005.
10. L. Roche, M. Pelletier, “Modelling of the thermomechanical and physical processes in FR fuel pins using the GERMINAL code”, Proceedings of Symposium on MOX fuel technologies for medium and long term deployment, IAEA-SM-358/25, IAEA, Vienna, 2000.
11. A. Marrel et al., « An efficient methodology for modelling complex computer codes with Gaussian processes », Computational Statistics and Data Analysis, 52, pp.4731-4744, 2008